Composites: Part A 172 (2023) 107597

Contents lists available at ScienceDirect

Composites Part A

journal homepage: www.elsevier.com/locate/compositesa

Simultaneous improvement of heating efficiency and mechanical strength of a self-healing thermoplastic polymer by hybridizing magnetic particles with conductive fibres

Zhao Sha [a], Xinying Cheng [a,b], Yang Zhou [a], Andrew N. Rider [c], Andrew D.M. Charles [c], Wenkai Chang [a], Shuhua Peng [a], May Lim [d], Victoria Timchenko [a], Chun H. Wang [a,*]

[a] School of Mechanical and Manufacturing Engineering, University of New South Wales, Sydney, NSW 2052, Australia
[b] Institute of Photonics, Leibniz University Hannover, Hannover 30167, Germany
[c] Defence Science and Technology Group, 506 Lorimer Street, Fisherman's Bend, VIC 3207, Australia
[d] School of Chemical Engineering, University of New South Wales, Sydney, NSW 2052, Australia

ARTICLE INFO

Keywords:
Magnetic hysteresis loss
Eddy-current loss
Thermoplastic polymer
Synergistic improvement

ABSTRACT

Radio-Frequency (RF) induction heating is a versatile in-situ method for contactless heating of structures by utilizing either magnetic hysteresis loss or eddy-current loss mechanism. Achieving high heating efficiency without degrading mechanical properties is a major challenge. Herein, a RF induction compatible self-healing composite was developed by hybridizing iron oxides (Fe_3O_4) nanoparticles with carbon fibre veils (CFVs) in poly(ethylene-co-methacrylic acid) (EMAA), which could possess both high magnetic and electrical properties. Owing to the multiscale conductive networks built by Fe_3O_4 nanoparticles and CFVs, the electrical conductivity of the nanocomposite was found to be higher than the linear combination of the individual contributions, thus creating a synergistic improvement in electrical conductivity and heating efficiency. Furthermore, single lap shear test results demonstrated that the combination of Fe_3O_4 nanoparticles and CFVs could significantly improve the bonding strength of EMAA polymer. Therefore, the hybridization of magnetic particles with conductive fibres offers a promising technology for a wide range of applications, such as self-healing, reversable bonding, and multiple use bonded composites.

1. Introduction

Radio-Frequency (RF) induction heating by either magnetic hysteresis or eddy-current is a versatile method for a wide range of applications, including hyperthermia treatment [1], self-healing [2], rapid repairs of structures [3,4], reversible joining and attachment [5], and curing of polymer composites [6]. The heating is generated by either of the two mechanisms: hysteresis loss of magnetic materials and eddy-current resistive heating of electrically conductive materials; the power of heating is proportional to volumetric fraction of the embedded magnetic or conductive materials in the composite. As these two mechanisms operate independently in linear systems, adding both magnetic and conductive materials results in the total heating power being the summation of their individual contributions [7,8]. Moreover, since the mechanical properties of the nanocomposite, such as strength, tend to decrease as more magnetic or conductive materials are added, it remains a major challenge to achieve high power heating without adversely affecting the mechanical properties.

RF induction heating can also directly heat self-healing and reversible adhesives in areas of interest, offering significant advantage over other external heating methods, such as heat guns, heating blanket or IR lamps, which deliver thermal flux by conduction through the thickness. The rates of heating of conventional methods are limited by many factors such as the permissible surface temperature, thermal conductivity, and thermal capacity of the host structure. Compared to other localized heating techniques such as resistance joule heating [9,10,11], and ultrasonic heating [12,13,14], the RF induction heating method [15,16,17,18] shows a great potential for contactless and wireless heating of thermoplastic adhesives, regardless of whether the composite structures to be bonded are thermoplastic or thermoset [19]. By modifying thermoplastic polymers to attain additional functionalities, such as magnetic or electrical conductivity, they can be heated by focusing the electromagnetic wave on the target area to perform healing or bonding without overheating surrounding structures.

* Corresponding author.

https://doi.org/10.1016/j.compositesa.2023.107597
Received 15 November 2022; Received in revised form 11 April 2023; Accepted 30 April 2023
Available online 6 May 2023

To generate heat directly from within the thermoplastic polymers by applying an alternating magnetic field, magnetic particles have been embedded [20]. For instance, ferrimagnetic Fe_3O_4 nanoparticles, which feature a high magnetic hysteresis loss, can generate heat upon the application of an alternating magnetic field [21]. Although Fe_3O_4 nanoparticles have shown great potential to act as heating sources under magnetic field in these works, they have been applied to thermoplastic polymers with low bond strength. Ciardiello et al.[22] embedded Fe_3O_4 nanoparticles in a polypropylene copolymer to develop an adhesive that can be heated by an external alternating magnetic field. Although the adhesive showed a relatively quick heating rate, the maximum bond strength only reached 2.0 MPa. Similar work conducted by Salimi et al. [23] reported an adhesive made of polyurethane (PU) and Fe_3O_4 nanoparticles, which also exhibited a relatively low shear strength of ~1.4 MPa. These reported bond strengths were considerably lower than those of structural adhesives [24,25] that can achieve bond strengths greater than 10 MPa.

One promising thermoplastic material with excellent bond strength and self-healing characteristics is poly(ethylene-methacrylic acid) (EMAA) [26,27], which features high toughness, low melting point and high melt flow index. With the ability to undergo hydroxyl-acid condensation reactions, catalysed by tertiary amines, many thermoset polymers can generate volatile by-products during cure [28,29]. However, EMAA has been found to be an excellent candidate to heal cracks in composites, especially when these volatile by-products can coalesce within the EMAA phase to form high pressure microbubbles, which can help drive the molten EMAA to fill the gaps and cracks inside the composites [30,31,32]. In our recent work [5], EMAA was used as the matrix for ferrimagnetic Fe_3O_4 nanoparticles to develop a reversible nanocomposite adhesive that could be heated to above the melting temperature by an external alternating magnetic field. The bonding strength of the EMAA/Fe_3O_4 nanocomposite adhesive was found to reach 8.2 MPa. However, one drawback is the low heating power, limiting the applicability to only polymers of low melting temperatures. Recently, several research investigations have reported that adding conductive fillers like graphene nanoparticles (GNPs) [33] to iron oxide particles have improved the heating performance by capitalizing on both magnetic hysteresis loss and eddy-current heating mechanisms.

One major issue with combining magnetic and conductive phases is that the specific heating efficiency (heating power per unit weight of fillers) remains largely unchanged, because the magnetic hysteresis and eddy-current heating mechanisms operate independently and are linearly additive. However, certain magnetic nanomaterials, such as Fe_3O_4 [34], are known to be also electrically conductive albeit their conductivity is much lower than metals. This dual characteristic creates an interesting possibility of improving specific heating efficiency by exploring the interactions between electrically conductive magnetic materials and highly conductive materials. To this end, we have selected Fe_3O_4 nanoparticles as the conductive magnetic phase and carbon fibre veils (CFVs) as the high conductivity phase to be embedded in poly (ethylene-methacrylic acid) (EMAA) matrix. The key questions are whether the interaction of the two different phases yields an additive or synergistic effect and whether they can simultaneously enhance specific heating efficiency and bond strength.

2. Experimental details

2.1. Materials

Poly(ethylene-co-methacrylic acid) (EMAA, Sigma-Aldrich) pellets with a melting temperature of 76 °C were selected as the thermoplastic polymer in this study. Iron (II, III) oxide nanoparticles (Fe_3O_4, Sigma-Aldrich) with a diameter between 50 and 100 nm were used as the dual-functional fillers for localized heating and structural reinforcement of the polymer. The electrical conductivity of Fe_3O_4 is about 3.33×10^3 S/m [35]. Carbon fibre veil (CFV, Fibre Glast Developments Corporation) with an areal density of 6.8 g/m^2 and a thickness of ~0.05 mm was chosen to incorporate with Fe_3O_4 nanoparticles to improve the bonding strength and magnetic heating performance of the nanocomposite. The electrical conductivity of carbon fibre is about 5.56×10^4 S/m according to the product datasheet.

2.2. Preparation of EMAA films reinforced with CFV and Fe_3O_4 nanofillers

EMAA pellets were first ground into powder by using a cryogenic grinder (Freezer Mill 6870, SPEX Sample Prep LLC); the particles approached their average size around 250 μm after three grinding cycles of 3 mins with 3-min intercooling after each cycle. The reason for implementing this process is to achieve a relatively uniform distribution of Fe_3O_4 nanoparticles in the EMAA film, as the EMAA particles act as carriers for the iron oxide nanoparticles during hot press forming. The finely ground EMAA particles were then mixed with Fe_3O_4 nanoparticles at varying weight ratios using a high-speed mixer (FlackTek SpeedMixer): i.e., 1.0 wt%, 5.0 wt%, 10.0 wt%, 20.0 wt% and 30.0 wt%. The resultant mixtures were spread out uniformly on CFVs with the assistance of a blade and then thermoformed into composite films of 0.3 mm thickness using a hot press (Carver 4386 CH) at 90 °C for 10 min. The pressure was controlled to be around 1000 psi. A sketch of the fabrication process is shown in Fig. 1. The introduction of Fe_3O_4 nanoparticles can enhance the conductivity of CFV-reinforced EMAA film. In particular, the Fe_3O_4 nanoparticles formed localised conductive clusters that connect adjacent carbon fibres, as illustrated in Fig. 1, creating a synergistic improvement between the conductive networks of the CFs and the Fe_3O_4 nanoparticles. The enhancement in the conductivity of the hybrid composite film results in better inductive heating performance. Pristine EMAA films as well as EMAA films reinforced only by CFV or Fe_3O_4 nanoparticles were fabricated under the same condition for comparative study. To eliminate the interference from possible non-uniform distribution of Fe_3O_4 nanoparticles, electrical, thermal, and mechanical characterization tests were carried out on samples away from the edge area of the thermoformed EMAA films.

2.3. Characterizations

2.3.1. Microscopy and spectroscopy characterization

An optical microscope (ZEISS Axio Zoom V16) was used to characterize the surface morphology of the cryogenic ground EMAA particles before and after mixing with Fe_3O_4 nanoparticles. The distribution of EMAA particle size was studied through a laser diffraction particle size analyzer (Mastersizer 3000, Malvern). A scanning electron microscope (FEI Nova NanoSEM 450) was used to characterize the surface morphologies of pristine EMAA particles, Fe_3O_4-coated EMAA particles, CFV, cross-section of adhesives films, and fracture surfaces of single lap shear test samples. To study the distribution of Fe_3O_4 nanoparticles and CFV inside EMAA films, samples were potted in a mounting epoxy resin first and then cut into thin slices by microtome for transmission electron microscopy (TEM) observation with a 200 kV field emission TEM (JOEL FEG 2100F). X-ray Diffraction (XRD) patterns of pristine EMAA, EMAA/Fe_3O_4, EMAA/CFV/Fe_3O_4 films were collected on a Cu-source XRD instrument (Aeris, Malvern Panalytical).

2.3.2. Bond strength

One major application of the EMAA based nanocomposites containing Fe_3O_4 nanoparticles and CFVs is reversible adhesives for rapid bonding and debonding of structures. The bond strength of adhesive films was measured using a single lap-shear test method; tests were conducted using an Instron 3369 universal testing machine with a 10 kN load cell at room temperature. To quantify the bond strength of the EMAA/Fe_3O_4/CFV nanocomposite adhesive, two adherends made of unidirectional carbon fibre reinforced epoxy laminates (25 mm × 50 mm × 1.6 mm) were bonded by the EMAA based adhesive using a hot

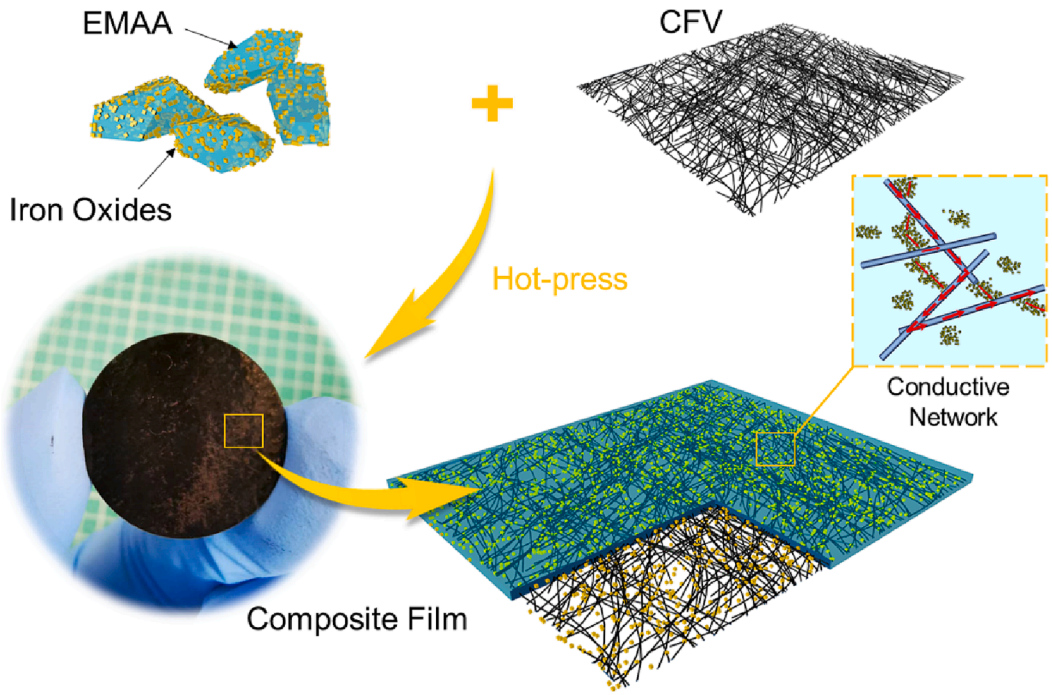

Fig. 1. Schematic illustration of the fabrication approach for EMAA/CFV/Fe_3O_4 composite film.

press (Carver 4386 CH) at a pressure of 1 MPa for 10 mins after the adhesive was heated to its melting temperature. The nominal overlap area of the single lap shear test samples was controlled to be 25 mm × 12.5 mm. During single lap shear tests, the crosshead displacement rate was set to be 1 mm/min according to the ASTM D3165. The lap-shear strength was calculated from the tensile force per unit overlap area. Samples were repeatedly disbonded and rebonded five times to investigate the strength retention performance, which is critical to self-healing and reversible bonding.

2.3.3. Electrical conductivity

Electrical conductivity measurements were performed on the EMAA based polymer composite films to characterize changes in their in-plane and through-thickness conductivity due to the introduction of CFV and Fe_3O_4 nanoparticles. For in-plane conductivity measurement, composite films were cut to the size of 40 mm × 5 mm, and conductive a silver paste was applied at the ends of the samples to attach copper wires needed for the measurement. For the through-thickness electrical conductivity, the composite films were cut to circular discs with a diameter of 10 mm, which were then held tightly between two flat stainless-steel plates by an electrode clamp. The copper wires and electrode clamp were eventually connected to a Keysight 34465A digital multimeter to measure the resistance, and the electrical conductivity, σ, was calculated using the following equation: $\sigma = L/RA$, where L denotes the length of the sample between the electrodes or the through thickness of the sample, R the measured electrical resistance (Ω), and A the cross-sectional area (m^2).

2.3.4. Electromagnetic heating performance

An induction heating system (EASYHeat 0224, Ambrell, US) was used to generate an alternating magnetic field at 189 kHz. The spiral coil was 32 mm in length with eight turns. The coil had a hollow rectangular cross section to allow cooling water to pass through, and the cross-section area of water-cooling path was approximately 1.3 mm × 5.3 mm. In this study, different currents with a range from 100 A to 300 A were applied to generate magnetic flux of varying intensities. To measure the magnetic heating performance, the nanocomposite adhesive films were cut into circular discs and placed on a square fibreglass composite, which was mounted on the top of the spiral coil. The distance between the nanocomposite adhesive film and coil was 2 mm, the same as the thickness of the fibreglass laminate. The temperature changes of the adhesive films with time under alternating magnetic fields were monitored using an infrared camera (FLIR X6540sc).

3. Results and discussion

3.1. Microstructure

An optical microscopy image of typical cryogenically-ground EMAA particles is shown in Fig. 2a. The EMAA particles are generally of a size of ~250 μm, and their size distribution is shown in the inset of Fig. 2a. Fig. 2b shows an SEM image indicating the surface morphology of cryogenically ground EMAA particle, whose surface appears relatively flat and clean, which is typical of brittle fracture at the cryogenic temperature. After being successfully coated with iron oxide nanoparticles, with the assistance of a high-speed mixer, the EMAA particles change from transparent to black, as shown in Fig. 2c. Fig. 2d shows an SEM image of the iron oxide nanoparticles coated on one EMAA particle, where a large number of iron oxide nanoparticles with a size between 50 and 100 nm can be clearly observed. The CFVs used in this study consist of carbon fibres with a diameter of ~7 μm, as shown in Fig. 2e and 2f. The thickness of CFV is only about 50 μm, resulting in a relatively good transparency, as shown in the inset of Fig. 2e.

Fig. 3a shows the measured hysteresis loop of iron oxide nanoparticles coated EMAA powder. The energy spent in reversing the magnetization of the material converts to heat, which is known as the hysteresis loss and is proportional to the area of the hysteresis loop [36]. XRD spectra of three different adhesive films are shown in Fig. 3b. For the pristine EMAA adhesive, two characteristic peaks can be observed between 2θ = 20–30°, which agree well with the previously reported XRD spectrum of EMAA [37]. After adding iron oxide nanoparticles, the characteristic peaks of the EMAA/Fe_3O_4 became less obvious compared to the peaks of iron oxides, which was attributed to the stronger response of iron oxide crystalline grain during the XRD measurement. According to a previously reported study [38,39], several characteristic peaks of iron oxides can be identified, as shown in the red curve of

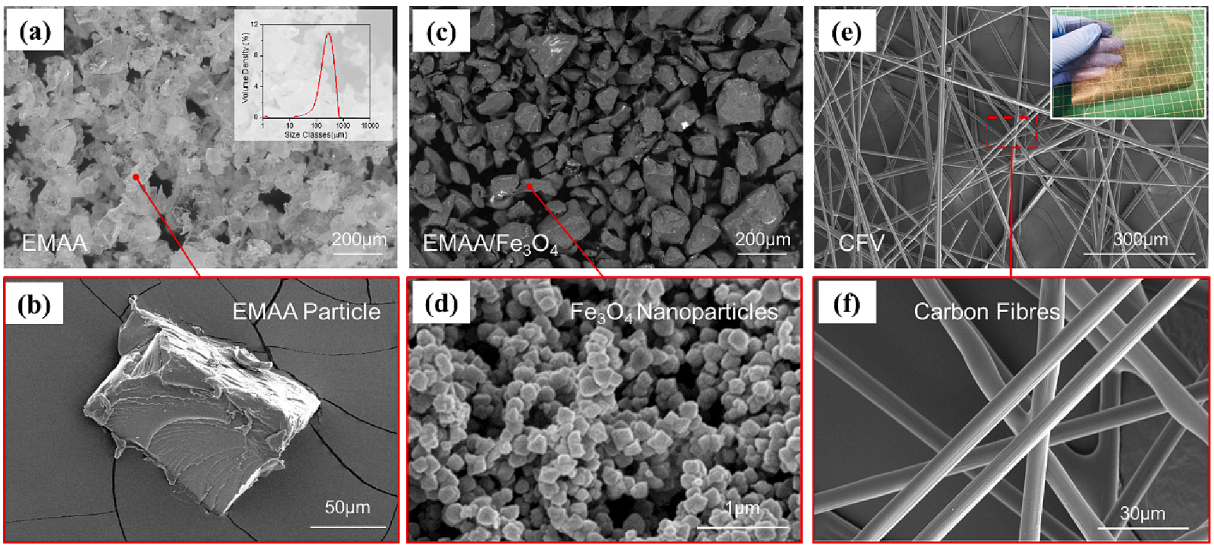

Fig. 2. Morphologies of EMAA, Fe_3O_4 nanoparticles and CFV: (a) Optical microscopy image of cryogenically ground pristine EMAA powder, the inset shows the particle size distribution; (b) typical surface morphology of pristine EMAA particles; (c) optical microscopy image of Fe_3O_4 nanoparticles coated EMAA powder; (d) SEM image of Fe_3O_4 nanoparticles on EMAA surface; (e) SEM image of CFV used in this study, the inset shows a digital photography of CFV, and (f) an enlarged view of carbon fibres.

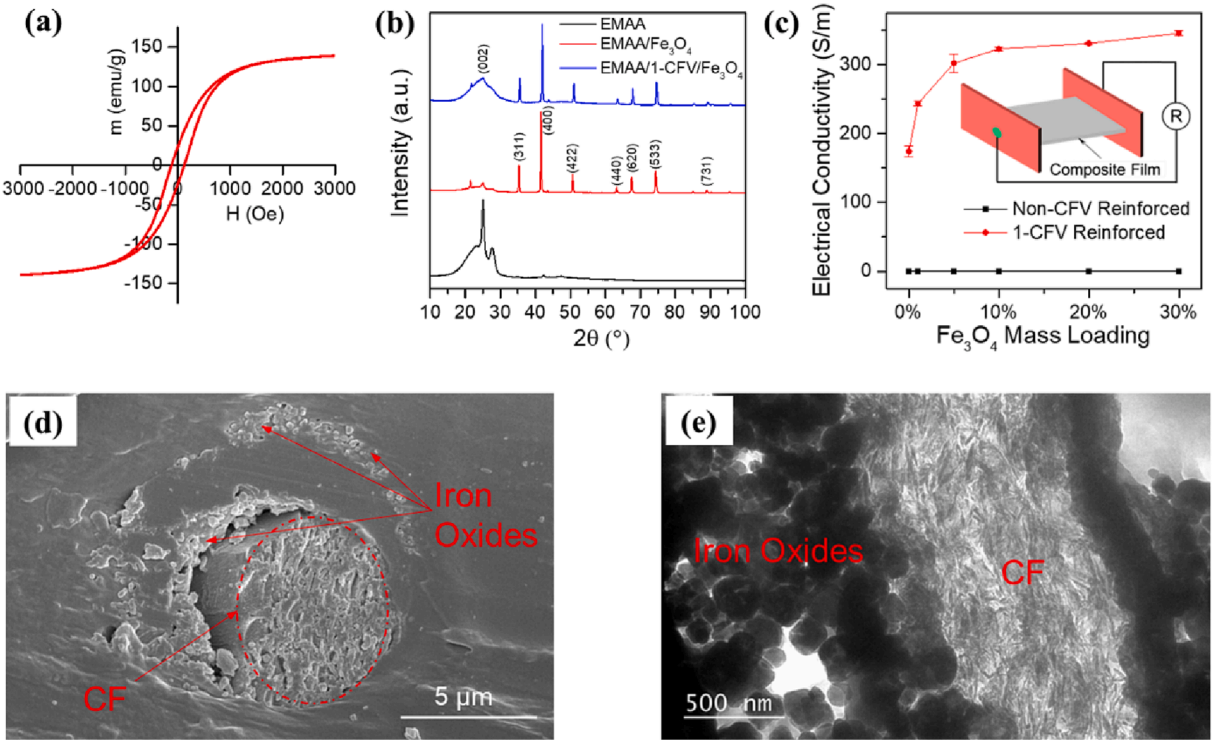

Fig. 3. Material properties characterizations: (a) Hysteresis loop of iron oxide nanoparticles coated EMAA powder, (b) XRD spectra of three different adhesive films, (c) In-plane electrical conductivity measurement results on adhesives with and without CFV, (d) cross section SEM and (e) TEM images of EMAA/CFV/Fe_3O_4 adhesive.

Fig. 3b. Further introduction of CFV in the adhesive led to stronger peaks at around $2\theta = 26°$, which is the characteristic peak of carbon C (002).

The in-plane electrical conductivities of EMAA/Fe_3O_4 with different iron oxide mass loadings and reinforced with a single layer of CFV are shown in Fig. 3c. It can be clearly seen that without CFV the EMAA/Fe_3O_4 remains non-conductive, even with the highest mass loading (30 wt%) of iron oxide nanoparticles, indicating that a percolating conductive network was not formed for an iron oxide nanoparticle loading of 30% in EMAA. By contrast, incorporating one layer of CFV in the EMAA dramatically improved the conductivity to 174 S/m, attributed to the high conductivity of the CFV. However, combining iron oxide nanoparticles with CFV together yielded significant improvement in the in-plane electrical conductivity, as shown by the red curve in Fig. 3c. The electrical conductivity increases rapidly with the weight loading of iron oxide nanoparticles.

The electrical conductivity improvement made by iron oxide nanoparticles was initially significant at low mass loadings, and finally reached a steady state at the highest mass loadings. According to the

conductivity measurement, adding 30 wt% iron oxide nanoparticles in one-layer CFV reinforced EMAA adhesive doubled the in-plane electrical conductivity to about 346 S/m compared to CFV only. While this significant improvement in electrical conductivity, by the combination of CFV and iron oxide nanoparticles, is consistent with the general rule that conductive fillers improve the conductivity of polymers, the synergistic improvement is a surprising finding. The large difference between the two sets of results presented in Fig. 3(c) indicates a significant synergy between the CFVs and Fe_3O_4 nanoparticles, which by themselves are insufficient to form a percolating conductive network [40] because the iron oxide nanoparticles alone were found to have no observable effect on conductivity. It is noted that the fabrication method applied in this study has the possibility of creating non-uniform distribution of conductive network within the composite film. However, this kind of non-uniform distribution generally occurs at a scale comparable to the size of the EMAA particles, around 250 μm. At the millimetre scale, the conductive network is highly uniform within the composite film. To validate this, additional conductivity measurements were conducted on EMAA/1-CFV/30 wt% Fe_3O_4 samples of varying sizes (5 mm × 5 mm, 10 mm × 5 mm, 20 mm × 5 mm, and 40 mm × 5 mm), as shown in Fig. S1. The results show a high level of consistency in terms of electrical conductivity across all sample sizes, indicating that the conductive network is uniformly distributed within the composite film at a scale as small as 5 mm. Moreover, the electrical conductivity measurement results in Fig. 3c show that the error bars are not significant compared to the conductivity values, confirming the relatively uniform distribution of the conductive network across a large area.

Detailed examination of the distribution of iron oxide nanoparticles revealed that they were well dispersed in the EMAA matrix as shown by the SEM image of the cross section of the adhesive in Fig. 3d. TEM observation on a thin slice of adhesive film, as shown in Fig. 3e, shows that some iron oxide nanoparticles, which were a cubic shape, with sizes

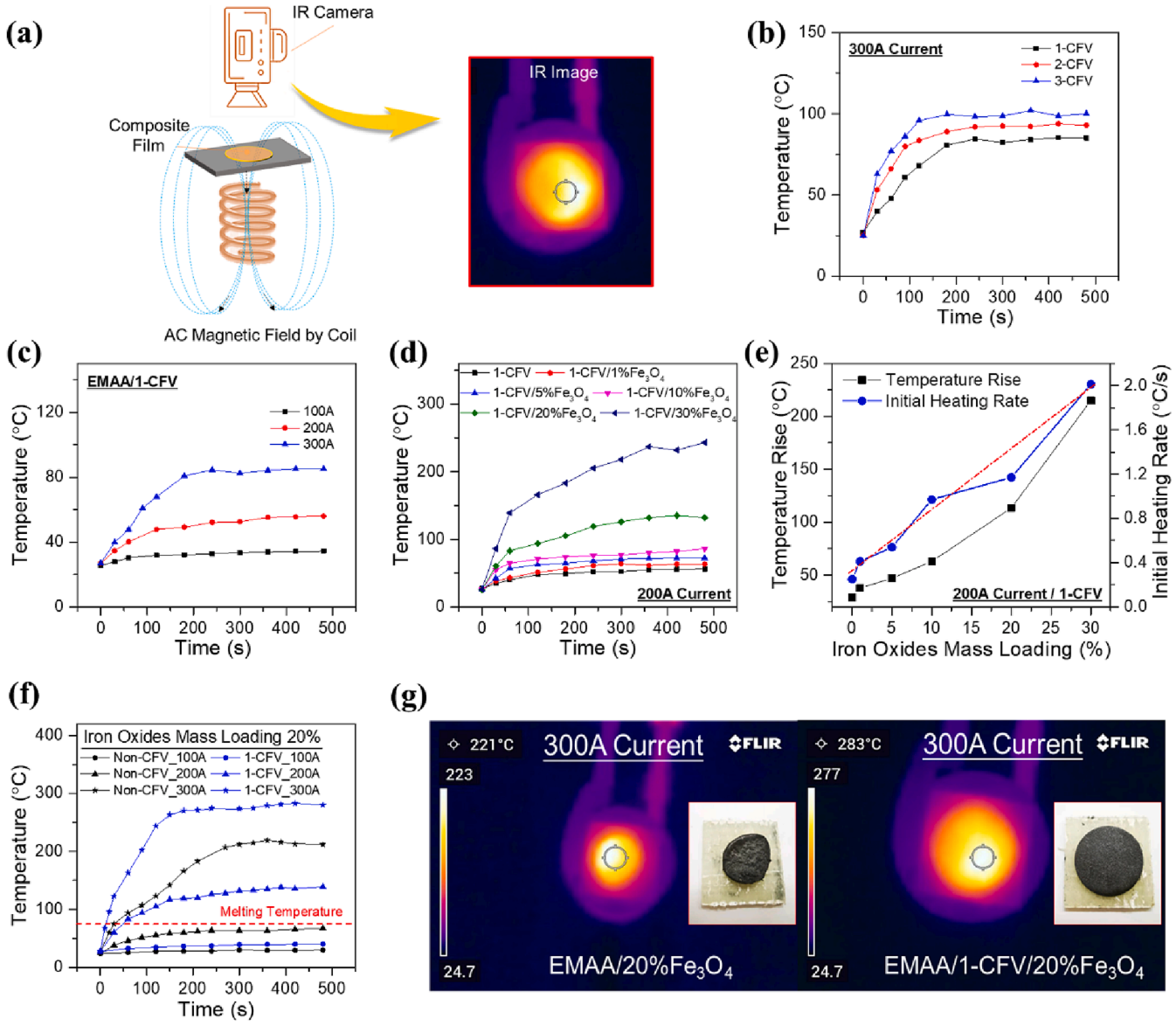

Fig. 4. Heating performance results: (a) Schematic of the induction heating process; The induction heating performance of (b) EMAA polymer film reinforced by different layers of CFV with an induction current of 300A, (c) EMAA/1-CFV composite film under different induction current, and (d) EMAA/1-CFV composite films with different iron oxide nanoparticles mass loadings under an induction current of 200A; (e) The influence of iron oxide nanoparticles mass loadings on temperature rise and initial heating rate of 1-CFV reinforced EMAA composite film; (f) Comparison of the induction heating performance between EMAA/20 % Fe_3O_4 and EMAA/1-CFV/20 %Fe_3O_4 composite films under different induction currents; (g) IR and digital images of EMAA/20 % Fe_3O_4 and EMAA/1-CFV/20 %Fe_3O_4 composite films at the stable state.

around 100 nm, were clustered along a ring that was likely the remnant of the surface of an EMAA granule on which the iron oxide particles were coated. Although the hot forming process deformed EMAA granules, the iron oxide nanoparticles remained concentrated and formed a segregated network. Even though the iron oxide nanoparticles are less conductive than carbon fibres, the segregated network provided conduction pathways that connect adjacent carbon fibres, as the cell size of the segregated network of iron oxide nanoparticles is much larger than the mean distance between carbon fibres. As a result, the in-plane electrical conductivity of the nanocomposite increased significantly above the linear summation of the separate conductivity increase due to the iron oxide nanoparticles and the carbon fibres.

3.2. Induction heating performance of EMAA based adhesive films

EMAA based polymer composite films were supported by a glass fibre reinforced composite laminate and inductively heated in an alternating magnetic field. The temperature change of the polymer film was monitored through an IR camera using the test setup shown in Fig. 4a. EMAA polymer films reinforced by up to three layers of CFV were also inductively heated with a current of 300A and a frequency of 189 kHz to investigate the influence of CFV on the adhesive's induction heating performance. As shown in Fig. 4b, increasing the number of CFV layers in the EMAA film from one to three can increase the heating rate and the maximum achievable temperature in the presence of convection cooling at one surface of the adhesive. However, the improvement in heating rate and the maximum achievable temperature are not proportional to the number of CFV layers. When the number of CFV layers increased from one to three, the final temperature rise of polymer film with 300A induction current only increases from 58 °C to 75 °C.

Compared with iron oxide nanoparticles of similar volume fractions, CFV seems to be less efficient in terms of the maximum temperature rise and the initial heating rate, as shown in Fig. S2a and S2b. Although both are inductively heated by the alternating magnetic field, the heat generated by these two components stemmed from different heating mechanisms. In an alternating magnetic field, the heat generated by CFV rely on the induced eddy currents, whereas for the iron oxide nanoparticles, heat was generated through hysteresis loss, with the power produced by each mechanism being described by the following expressions.

$$P_e = \frac{\pi^2}{4\rho} B_m^2 f^2 r^2 = \frac{\pi^2}{4\rho} \mu_{c1}^2 H_m^2 f^2 r^2 \quad (1)$$

$$P_h = \oint f B dH = \pi H_m^2 \mu''_{c2} f \quad (2)$$

where P_e and P_h denote to the eddy current loss (W) and hysteresis loss (W), respectively; ρ denotes the resistivity of carbon fibre, B_m the maximum flux density (T), H_m the maximum magnetic field strength (A/m), f the frequency of magnetic reversals per second (Hz), and r the radius of composite film here (m). Detail derivation process of the eddy current loss formula in conductive round shape film can be found in Supplementary Note 1, and the formula of hysteresis loss is from Ref. [5]. In these formulae, all the magnetic permeabilities are referring to the real value. μ_{c1} is the magnetic permeability of CFV reinforced EMAA composite film, which is very close to the value of magnetic permeability of vacuum ($\mu_0 \approx 1.256 \times 10^{-6}$H/m). μ''_{c2} is the imaginary part of magnetic permeability of iron oxides reinforced EMAA composite film, which is calculated using a simple linear model based on the volume fraction of iron oxide nanoparticles, and the EMAA is considered to have zero imaginary permeability during the calculation:

$$\mu''_{c2} = V_{Fe_3O_4} \times \mu''_{Fe_3O_4} \quad (3)$$

where V_{Fe3O4} denotes the volume fraction of iron oxide nanoparticles, and $\mu''_{Fe_3O_4}$ is the imaginary part of magnetic permeability of iron oxide nanoparticles. According to the formulae of these two losses, under the same magnetic field condition, the eddy current loss is not only related to the electrical conductivity of sample, but also to the size of the sample, while the hysteresis loss is only related to the sample's imaginary part of magnetic permeability. It is noted that in this study we have only investigated one particular Fe_3O_4 nanoparticle and carbon fibre veil. Their physical dimensions, such as the size of the particles, can potentially affect the mechanical property and heating performance of EMAA film, which could be the subject of future research.

The heating performance of a one-layer CFV reinforced EMAA film under different induction currents is shown in Fig. 4c. The maximum temperature and initial heating rate increased with induction current. However, as discussed previously, CFV alone demonstrated a limited heating performance: the maximum temperature (85.1 °C) achieved with a 300A induction current was only slightly higher than EMAA's melting point (76 °C), while the other two induction currents (100A and 200A) failed to melt EMAA. By contrast, the introduction of iron oxide nanoparticles into the 1-layer CFV reinforced EMAA significantly improved the heating performance. The heating performances of iron oxide nanoparticles ranging from 1.0 wt% to 30.0 wt% are shown in Fig. 4d. At the high mass loading of iron oxide nanoparticles (e.g., EMAA/1-CFV/30 wt% Fe_3O_4) the nanocomposite can be heated to 241 °C using an induction current of 200 A. This significantly enhanced heating performance stems from the synergistic improvement in electrical conductivity from the hybridization of iron oxide nanoparticles and one-layer of CFV.

The effect of iron oxide nanoparticle mass loading on the maximum temperature rise and the initial heating rate are shown in Fig. 4e. The result suggests both the maximum temperature rise and the initial heating rate increased approximately proportionally to the iron oxide mass loading. The bonding strength of joints made of EMAA/Fe_3O_4/CFV nanocomposites reveal that one-layer CFV together with 20 wt% iron oxide nanoparticles produced the best result, as discussed in Section 3.4, as well as the good heating performance. Consequently, the one-layer CFV/20 wt% iron oxide nanoparticles reinforced EMAA nanocomposite film was selected for further investigation under different currents, as shown in Fig. 4f. For comparison, the EMAA composite film with only 20 wt% iron oxide nanoparticles was also tested under the same condition. It can be clearly observed that owing to the existence of CFV, the heating performance of EMAA/1-CFV/20 %Fe_3O_4 is consistently better than that of EMAA/20 % Fe_3O_4 under any current. When the induction current is 300A, both composite films can be heated to above the melting point of EMAA. However, only the EMAA/1-CFV/20 %Fe_3O_4 film can reach the melting point of EMAA at a current of 200A. With the induction current of 100A, neither of the two films can be heated to above the melting point of EMAA, showing that this induction current value is insufficient for the practical application of contactless composites healing and reversible bonding technologies. Besides the heating performance improvement, adding CFV in the EMAA polymer film brings about additional benefit, as shown in Fig. 4g. When the temperature is above the melting point, the non-CFV reinforced EMAA composite film will shrink, and its original shape cannot be maintained. Comparatively, for the EMAA/1-CFV/20 %Fe_3O_4 film, even when it was inductively heated to as high as ~283 °C, its original shape can still be well maintained, owing to the structural support provided by the CFV. Such a benefit indicates that CFV can help maintain the structural integrity of polymer composite films, which is of great importance to the bonding process, since it ensures maintenance of the bonding area during induction heating of the EMAA polymer film.

To evaluate to contributions of CFV and iron oxide nanoparticles in improving the induction heating performance of EMAA polymer films, the initial heating rates of three composite films (EMAA/1-CFV, EMAA/20 wt% Fe_3O_4, and EMAA/1-CFV/20 wt% Fe_3O_4) under different induction currents were calculated, as shown in Fig. 5a. Specifically, the results of EMAA/1-CFV film and EMAA/20 wt% Fe_3O_4 film can reflect the individual contributions of CFV and iron oxide nanoparticles,

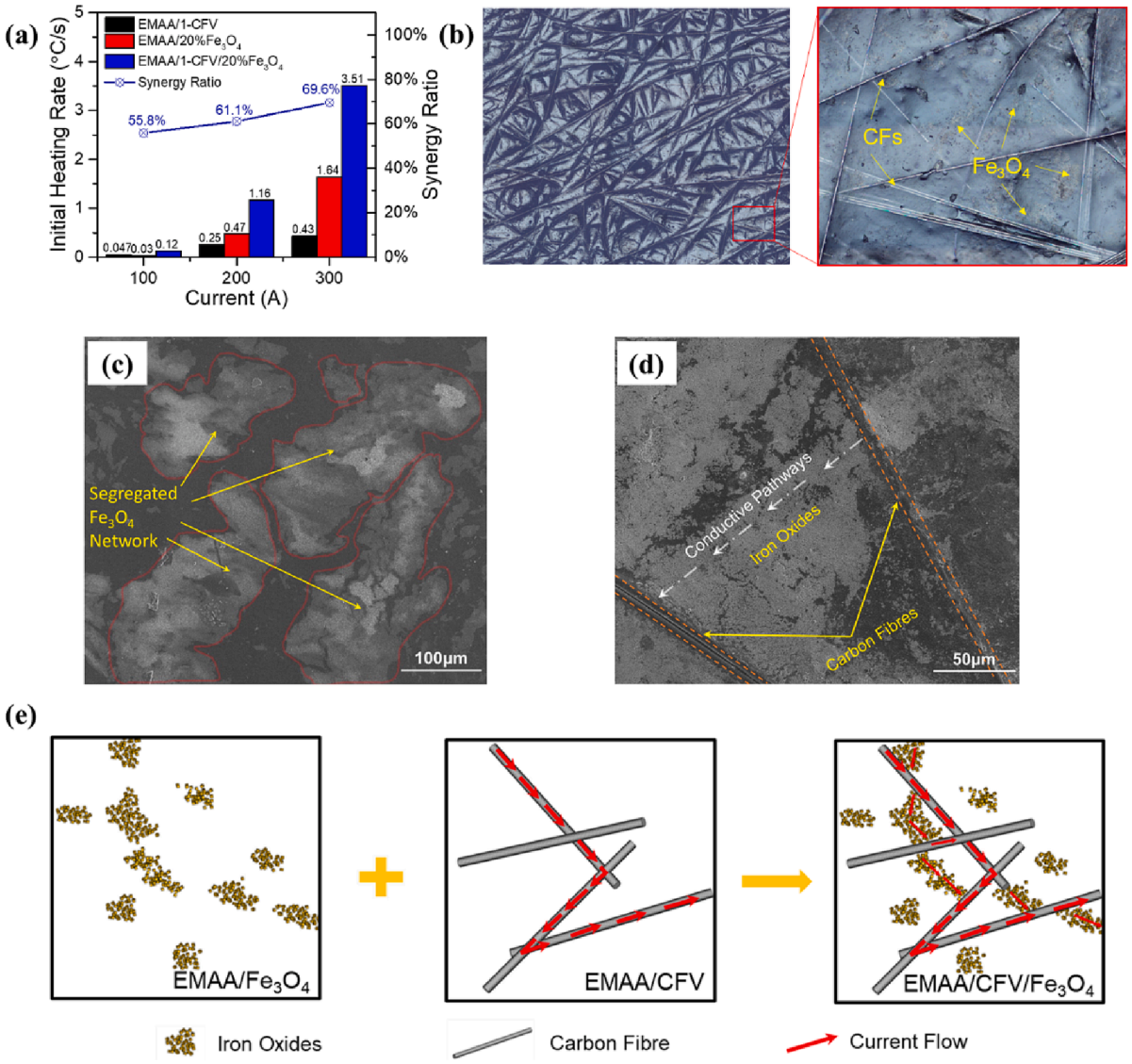

Fig. 5. Synergistic improvements:(a) Initial heating rate of three different polymer composite films and the synergy ratio of CFV and 20 wt% Fe_3O_4 in improving the heating performance of EMAA composite film under different induction currents. (b) Optical microscopy image of EMAA/CFV/Fe_3O_4 composite film, the enlarged view shows the distribution of Fe_3O_4 clusters inside the CFV; SEM images of (c) segregated iron oxides network, and (d) iron oxides between two carbon fibres. (e) Schematic explanation describing the additional conductivity improvement by incorporating Fe_3O_4 with CFV.

respectively, while the results of EMAA/1-CFV/20 wt% Fe_3O_4 film reflect the combined contribution of CFV and iron oxide nanoparticles in improving the induction heating performance of the adhesive. Basically, in terms of the initial heating rate, the combined contributions of these two materials are always significantly larger than the sum of their individual contributions. Therefore, it is worthwhile to calculate the synergy ratio of these two materials in improving the induction heating performance of the adhesive. The synergy ratio can be calculated using the method proposed in [41]:

$$S = \left(\frac{Q_{combined}}{Q_{CFV} + Q_{Fe_3O_4}} - 1\right) \times 100\% \quad (4)$$

where S is the synergy ratio of CFV and iron oxides nanoparticles in improving the induction heating performance of composite film; $Q_{combined}$ refers to the combined contribution of CFV and iron oxides nanoparticles, in terms of the initial heating rate; Q_{CFV} and Q_{Fe3O4} refer to the individual contributions of CFV and iron oxide nanoparticles, respectively. The calculated synergy ratios of CFV and iron oxides nanoparticles under different currents are shown in Fig. 6a. It can be seen that synergy ratio of CFV and iron oxide nanoparticles in improving the initial heating rate changes from 55.8 % to 69.6 % when the induction current increases from 100A to 300A. This synergistic improvement in the initial heating rate is most likely due to the improved electrical conductivity of the adhesive after combining CFV and iron oxide nanoparticles. Fig. 5b shows an optical microscopy image of the EMAA/CFV/Fe_3O_4 composite film, from the enlarged view, it can be clearly seen that multiple iron oxide nanoparticle clusters are distributed among the carbon fibres. This kind of morphology is owing to the specific preparation method applied in this study, which can create segregated iron oxide conductive networks inside the adhesive, as shown in Fig. 5c. Although there is another way to improve dispersion of iron oxide nanoparticles inside the adhesive, by dispersing iron oxide nanoparticles into EMAA dissolved THF solution, this does not improve heating performance and requires a very high iron oxide concentration to reach the percolation threshold for the adhesive to be electrically conductive. These segregated iron oxide networks created in this study are internally conductive, due to the EMAA insulating them from each other, and they are unable to form a conductive network inside the adhesive by themselves. However, with CFV, these segregated iron oxide

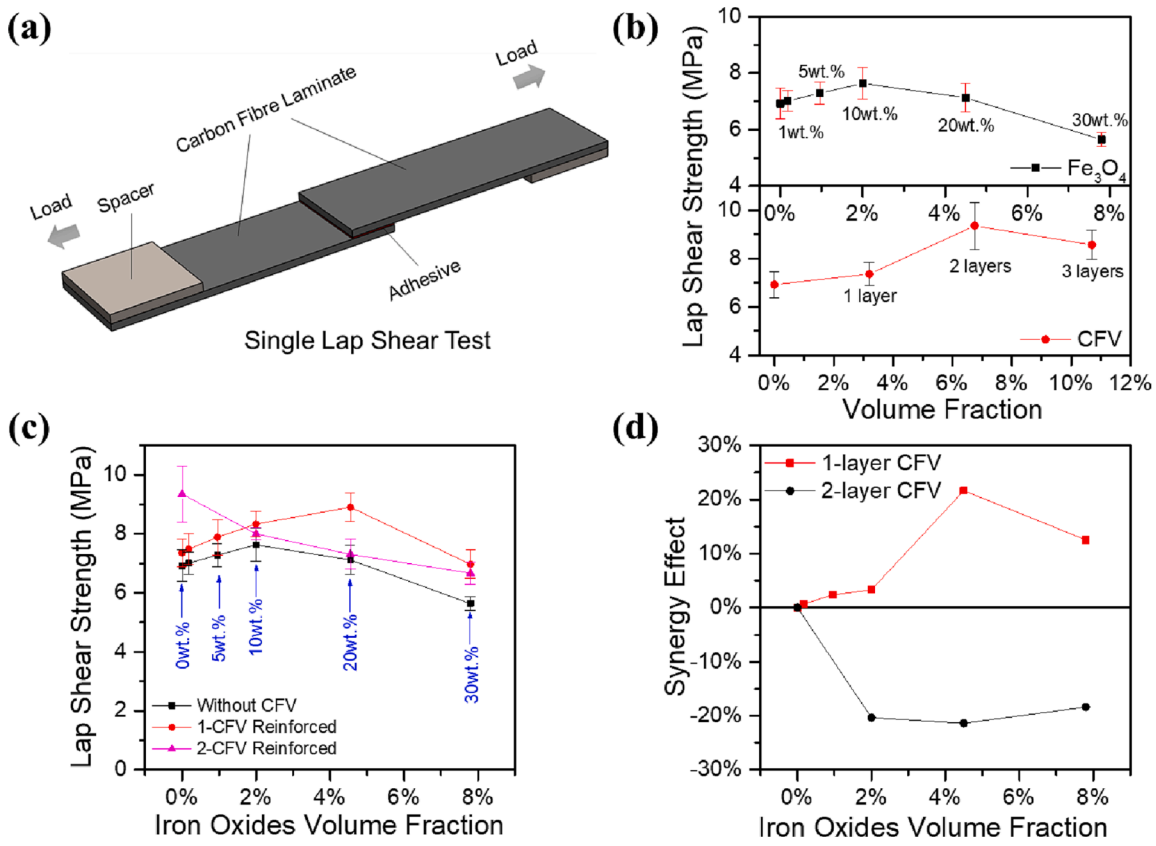

Fig. 6. Single lap shear test results:(a) Schematic of the single lap shear test specimen; (b) Plots of polymer film's lap shear strength against volume fractions of iron oxide nanoparticles and CFV; (c) Lap shear strength of 1-layer and 2-layer CFV reinforced EMAA composite films with different iron oxide volume fractions; (d) Synergy effect of 1-layer/2-layer CFV with different volume fractions of iron oxide nanoparticles.

networks are connected with each other, and they can also provide additional current flow pathways between different carbon fibres, as shown in Fig. 5d, thus further improving the electrical conductivity of the adhesive. A Schematic explanation describing the additional conductivity improvement is shown in Fig. 5e. A similar phenomenon has been reported in [42], where the additional electrical conductivity improvement was achieved by the combination of Fe_3O_4 and carbon nanotubes (CNTs). In this study, this additional electrical conductivity improvement made by iron oxide nanoparticles and 1-layer CFV helps to generate more heat through the eddy currents and leads to a higher initial heating rate.

3.3. *Effects of hybrid reinforcement on the bond strength*

The bonding strength of different EMAA based polymer composite films was characterized through a single lap shear test. The schematic of the single lap shear test specimen is shown in Fig. 6a, and the lap shear strengths were calculated by dividing the failure load by the bond area. Prior to investigating the combined effect of CFVs and iron oxides on the bonding strength of EMAA polymer film, the individual contributions were studied, as shown in Fig. 6b. By varying the number of CFV layers from 0 to 3, the lap shear strength of the EMAA polymer film increased first and then decreased, and the maximum strength was achieved with the 2-layer CFV reinforced composite film. The initial increase of bonding strength is likely owing to the CFV's strength reinforcement of the adhesive, while the final strength decrease may be attributed to the reduced volume fraction of EMAA, which may lead to a reduced effective bonding area on the test specimen. The addition of iron oxide nanoparticles exhibits a similar trend on the bonding strength of EMAA polymer films to the CFVs. The bonding strength increases from 6.92 MPa to 7.63 MPa when the mass loading of iron oxide nanoparticles in EMAA reaches about 10 %. Further increasing the iron oxide nanoparticle mass loading in EMAA leads to a decrease in the bonding strength, which is caused by the localized agglomerations of nanoparticles and has been revealed in our previous study [5].

To explore the co-effect of CFVs and iron oxide nanoparticles on the polymer film bond strength, EMAA composite films with various CFV layers and iron oxide mass loadings were prepared. The lap shear strength of 1-layer and 2-layer CFV reinforced EMAA composite films against various iron oxide mass loadings is shown in Fig. 6c, the results of EMAA composite films without CFV are also displayed to make a comparison. For the 1-layer CFV reinforced EMAA composite film, the largest lap shear strength (8.91 MPa) was achieved with 20 wt% iron oxide, which was 28.8 % higher than that of the pristine EMAA polymer film. When compared with the results of non-CFV reinforced EMAA composite films shown in Fig. 3c, it is observed that the optimum mass loading of iron oxide nanoparticles in improving the bonding strength of adhesive has increased from 10 wt% to 20 wt%. For the 2-layer CFV reinforced EMAA composite film, the largest bonding strength was achieved with no addition of iron oxides, and the bonding strength decreased with the increase of iron oxide mass loading.

A generalized additive model of the relationship between lap shear strength and the volume fraction of iron oxides and CFV has been developed based on the strength curves in Fig. 6b, as shown in Supplementary Note 2. This model provides the prediction about lap shear strengths of samples with different iron oxides and CFV volume fractions, which is based on a principle of linear addition. A comparison of experimental values and model calculated values is shown in Fig.S4. It can be clearly seen that the calculated values of EMAA samples modified with pure iron oxides or pure CFV agree well with their experimental values. However, for the samples modified by 1-layer CFV and iron oxides, their results mostly locate at the top left area of the plot,

indicating a larger experimental lap shear strength than the calculated value. On the contrary, the results of samples modified by 2-layer CFV and iron oxides all locate at the bottom right area of the plot, suggesting that the calculated lap shear strengths are overestimated compared with the experimental values. Further comparison between the experimental and calculated lap shear strengths against the volume fraction of iron oxides can be found in Fig.S4. Basically, the combination of 1-layer CFV and iron oxide exhibits a positive synergistic improvement in the lap shear strength, while 2-layer CFV and iron oxides are interfering with each other, leading to a degradation of the lap shear strength, as shown in Fig. 6d. With these findings, it can be easily observed that incorporating 1-layer CFV with iron oxide nanoparticles is a better approach to improving lap shear strength.

To explore the strengthening mechanism by adding 1-layer CFV and iron oxide nanoparticles in the EMAA adhesive, the failure type of single lap shear test specimens was examined, as shown in Fig.S5. It can be clearly observed that for the pristine EMAA adhesive bonded specimen, the failure typically occurs interfacially. However, after adding iron oxide nanoparticles or CFV in EMAA adhesive, the failure gradually changes to a cohesive mode, which is expected to result in a higher bonding strength than the interfacial mode. Such a change in the failure mode is most likely due to the reinforcing effect of iron oxide nanoparticles and CFV, and it has previously been reported that the addition of nanoparticles in adhesive can result in a change in failure mode from interfacial to cohesive failure [43,44]. It is noted that for the specimen bonded by the 1-layer CFV and 30 wt% iron oxide nanoparticles reinforced EMAA composite film, that although the failure mode is predominantly cohesive, the bonding strength has decreased, which is caused by the agglomeration of nanoparticles in the adhesive at the higher mass loadings.

The fracture surfaces of single lap shear test specimens have been investigated through SEM technique to further explore the reinforcing mechanism of CFV and iron oxide nanoparticles on the bonding strength of EMAA composite film. Fig. 7a shows the fracture surface morphology of pristine EMAA polymer film bonded specimen. As the failure is interfacial, the fractured surface appears as an inverted mould of the of carbon fibre laminate surface morphology. Several carbon fibre pull-outs and fractures can be observed from the fracture surface for specimens bonded with the 1-layer CFV reinforced EMAA composite film, as shown in Fig. 7b, which may contribute to the bonding strength improvement. For specimens bonded by the 1-layer CFV/20 wt% Fe_3O_4 reinforced EMAA composite film, the carbon fibre reinforcing effect can also be observed on the fracture surface, as shown in Fig. 7c. Meanwhile, in the enlarged view of Fig. 7c, iron oxide nanoparticles can be clearly identified surrounding the carbon fibre, providing nanoscale reinforcement to the polymer composite film. However, as the mass loading of iron oxide nanoparticles in the composite film increases, more areas of high-volume iron oxide nanoparticles appear at the fracture surface of the specimen. This is observed in Fig. 7d, which shows the fracture surface of a specimen bonded by the 1-layer CFV/30 wt% Fe_3O_4 reinforced EMAA composite film. The enlarged view of Fig. 7d shows that a high concentration of iron oxide nanoparticles forms a porous structure around the carbon fibre, degrading the bonding between the EMAA and carbon fibre, as well as the bonding between the EMAA and the adherend (carbon fibre laminate). This type of localised agglomeration of iron oxide nanoparticles is the primary reason for the bond strength decrease in Fig. 6b and 6c at high iron oxide mass loadings.

The absolute and relative improvements of 1-layer CFV on the bonding strength of EMAA polymer composite films were investigated with different mass loadings of iron oxide nanoparticles to further explore the strengthening mechanism of CFV, as shown in Fig. 8a. It is observed that the CFV's significant (either absolute or relative) improvement on bonding strength was achieved with high iron oxide mass loadings (e.g., 20 wt% and 30 wt%), which may be related to the increased viscosity of the melted thermoplastic polymer after adding a high mass loading of iron oxide nanoparticles. It was reported previously that the carbon fibre reinforcements exhibit a more significant improvement of the mechanical properties of high melt viscosity film-type thermoplastic composites [45].

To comprehensively evaluate the mechanical properties and induction heating performances of composite films, experimental values of lap shear strength and initial heating rate of some samples in this study are plotted in Fig. 8b for comparison. To identify the optimum concentration of iron oxide nanoparticles, we propose a criterion that considers both mechanical and induction heating improvement as follows:

$$\eta = \frac{\Delta\sigma}{\Delta\sigma_{max}} \times \frac{\Delta k}{\Delta k_{max}} \tag{5}$$

where η represents the comprehensive performance index, $\Delta\sigma$ the increase in bonding strength over that of the pristine EMAA film, $\Delta\sigma_{max}$ the maximum increase among all samples, Δk the increase in the initial heating rate over the pristine EMAA film, and Δk_{max} the maximum value of the increase in the initial heating rate among all samples. The results are given in Table 1, indicating that the EMAA composite film with 1-layer CFV and 20 wt% iron oxides yields the highest comprehensive performance index value (0.1228) among all the combinations. Also, it is noted that the EMAA/1-CFV/20 wt% Fe_3O_4 composite film possesses

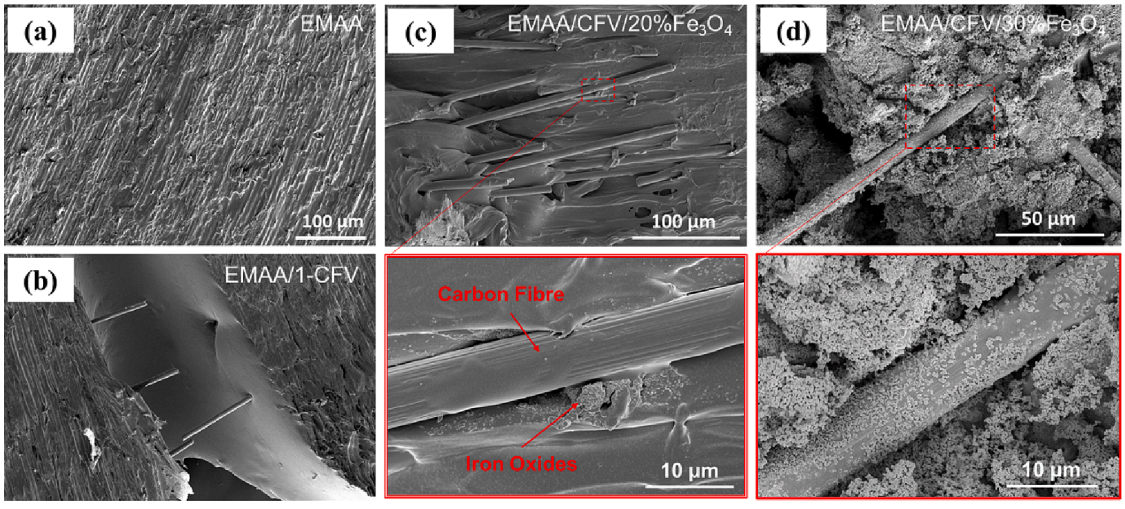

Fig. 7. Fracture surfaces of single lap shear test specimens bonded by (a) pristine EMAA adhesive, (b) 1-CFV reinforced EMAA adhesive, (c) 1-CFV/20 wt% Fe_3O_4 and (d) 1-CFV/30 wt% Fe_3O_4 reinforced adhesives.

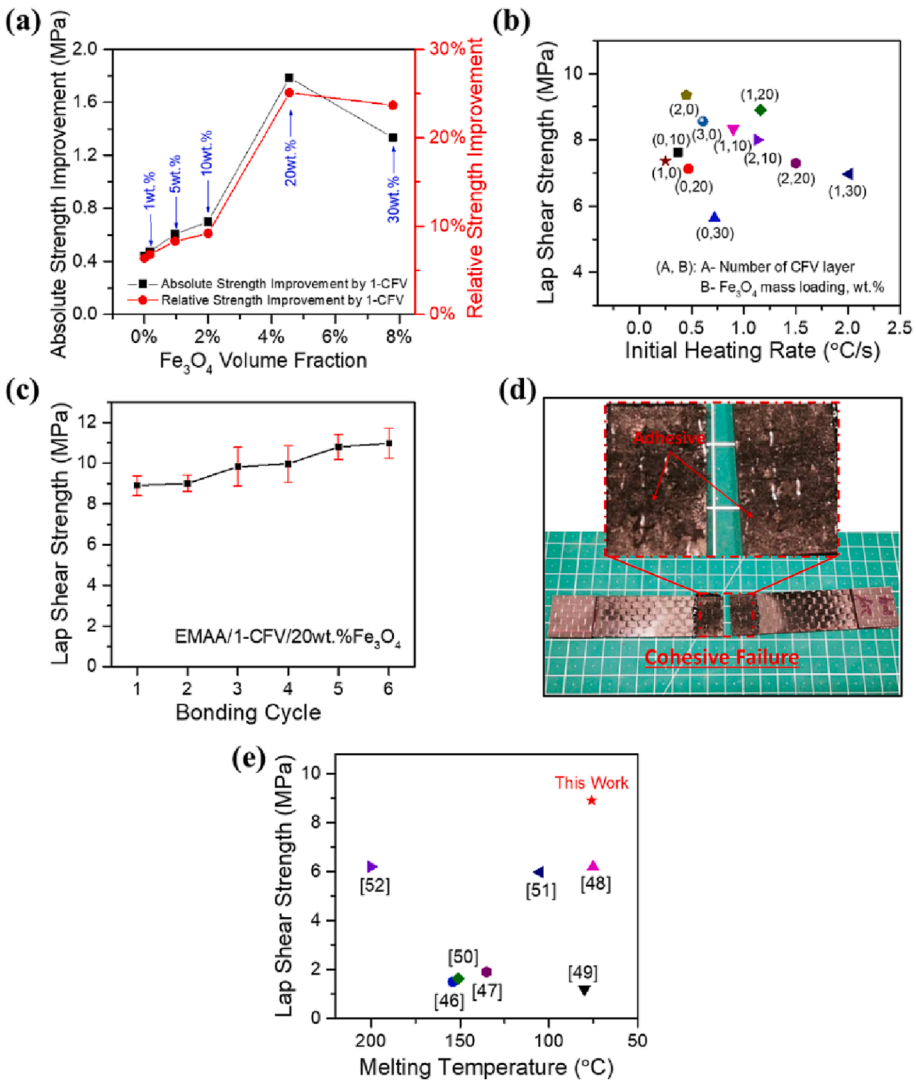

Fig. 8. (a) The absolute and relative strength improvement made by 1 layer of CFV with different iron oxide mass loadings; (b) Adhesive performance comparison in terms of lap shear strength and initial heating rate; (c) The bonding strength of 1-CFV/20 wt% Fe_3O_4 reinforced EMAA composite film *vs* bonding cycles; (d) Cohesive failure type of 1-CFV/20 wt% Fe_3O_4 reinforced EMAA composite film; (e) Adhesive performance comparison with literatures.

the highest lap shear strength among all other composite films that can be inductively heated to above the melting temperature under a medium strength induction current (200A), making it energy-efficient during the practical application.

For the reversible bonding technique, an essential property of the adhesive is the reusability. Single lap shear test specimens bonded by 1-layer CFV/20 wt% iron oxide nanoparticles reinforced EMAA composite film were selected to investigate the bonding performance after repeated debonding/rebonding (up to six) cycles, as shown in Fig. 8c. The bonding strength does not decrease after repeated debonding/rebonding cycles; instead, the bonding strength increases with the number of cycles. The measured bonding strength appears to reach a stable state at around 11 MPa after 5 debonding/rebonding cycles, and this strength increase is most likely due to the reduction of bond line thickness during the rebonding process [5]. Besides, after multiple debonding/rebonding cycles, the failure mode of specimen remains cohesive, as shown in Fig. 8d, indicating good bonding between the adhesive and adherend. These results demonstrate that the 1-layer CFV/20 wt% iron oxide nanoparticles reinforced EMAA polymer composite has an excellent reusability, with bond strength unaffected by repeated debonding/rebonding cycles. However, it is noted that although some of the composite films developed in this study do not exhibit the optimal performance, there are still potential areas of application for them. For instance, the EMAA/2-CFV/20wt.%Fe_3O_4 or EMAA/1-CFV/30 wt% Fe_3O_4 composite films could be applied in situations where a high induction heating rate is required, but moderate bonding strength is acceptable.

To objectively evaluate the performance of the EMAA composite film developed in this study, the lap shear strength and melting temperature of multiple thermoplastic adhesives were compared, as shown in Fig. 8e. These thermoplastic adhesives are from recently published studies, including polymers such as the commercial polyolefin based hot-melt adhesive (HMA) [46,47], ethylene vinyl acetate/aromatic hydrocarbon resin [48], poly(ethylene-co-butylene) [49], APOA/Polyolefin ester [50], natural rubber [51], and acrylonitrile butadiene styrene (ABS) [52]. It is noted that all these thermoplastic adhesives include both nanomaterial modified polymers and pure polymers. Through the comparison, it can be clearly observed that the EMAA polymer composite film developed in this study has a relatively low melting point, which is advantageous for portable, on-demand, and repeated composite healing and adhesion applications as it allows for a relatively shorter heating time than the other thermoplastic adhesives listed in Fig. 8d. Moreover, this EMAA based polymer composite film possesses the largest lap shear strength among these thermoplastic adhesives, which is

Table 1
Comprehensive performance index of different EMAA films.

Sample	Lap Shear Strength(σ, MPa)	Initial Heating Rate (k, °C/s)	Comprehensive Performance Index(η)
EMAAEMAA/10 wt% Fe_3O_4	6.927.63	00.37	00.0140
EMAA/20 wt% Fe_3O_4	7.12	0.47	0.0050
EMAA/30 wt% Fe_3O_4	5.64	0.72	−0.0490
EMAA/1-CFV	7.36	0.25	0.0059
EMAA/2-CFV	9.35	0.45	0.0582
EMAA/3-CFV	8.56	0.61	0.0532
EMAA/1-CFV/10 wt% Fe_3O_4	8.33	0.9	0.0675
EMAA/1-CFV/20 wt% Fe_3O_4	8.91	1.16	0.1228
EMAA/1-CFV/30 wt% Fe_3O_4	6.97	2.01	0.0053
EMAA/2-CFV/10 wt% Fe_3O_4	8	1.13	0.0649
EMAA/2-CFV/20 wt% Fe_3O_4	7.3	1.5	0.0303

Lap shear strength of pristine EMAA film $\sigma_0 = 6.92$ MPa. Initial heating rate of pristine EMAA film $k_0 = 0$ °C/s.
Lap shear strength improvement $\Delta\sigma = \sigma - \sigma_0$. Initial heating rate improvement:$\Delta k = k - k_0$.
$\Delta\sigma_{max} = 2.43MPa$, $\Delta k_{max} = 2.01^{\circ}\mathrm{C/s}$.

crucial for ensuring safe and reliable connections in composite structures.

4. Conclusion

In this work, an EMAA based polymer composite incorporated with carbon fibre veil and iron oxide nanoparticles was demonstrated to be a promising solution for the composite healing and reversible bonding applications. The EMAA based polymer composite exhibited a rapid heating performance under alternating magnetic field as well as excellent mechanical bond strength. Notably, the addition of a CFV in the polymer composite exhibited three functions: (i) constructing a conductive network inside the composite, which helps to significantly lower the effective percolation threshold for the iron oxide nanoparticles, leading to a higher initial heating rate of the composite; (ii) heating the composite to above its melting temperature with a lower induction current by the combined eddy-current and magnetic hysteresis loss mechanisms of the CFV and the iron oxides; and (iii) enhancing the lap-shear strength of the polymer composite under repeated debonding and rebonding. By incorporating 1-layer of CFV with 20 wt% Fe_3O_4 nanoparticles, the EMAA based polymer composite can be inductively heated to above its melting point in 20 s with an induction current of 300 A and a frequency of about 189 kHz, and its mechanical bonding shear strength can reach as high as 8.9 MPa, even after six repeated debonding/rebonding cycles. Such outstanding performance makes it possible for this polymer composite to be applied in a wide range of areas, including biomedical, electronic reuse, and recycling of bonded structures in the automotive and aerospace industry. The method of combining magnetic hysteresis loss with eddy-current heating has opened up a new avenue for developing high-performance composite healing agents or reversible adhesives for the future, and it can be extended to other types of thermoplastic polymers, thereby achieving a much wider range of applications.

CRediT authorship contribution statement

Zhao Sha: Conceptualization, Methodology, Investigation, Validation, Writing – original draft. **Xinying Cheng:** Conceptualization, Methodology. **Yang Zhou:** Methodology. **Andrew N. Rider:** Resources, Methodology, Writing – review & editing. **Andrew D.M. Charles:** Investigation. **Wenkai Chang:** Investigation. **Shuhua Peng:** Visualization, Writing – review & editing. **May Lim:** Resources, Methodology. **Victoria Timchenko:** Resources, Methodology. **Chun H. Wang:** Conceptualization, Methodology, Supervision, Writing – review & editing.

Declaration of Competing Interest

The authors declare that they have no known competing financial interests or personal relationships that could have appeared to influence the work reported in this paper.

Data availability

Data will be made available on request.

Acknowledgement

This research is Phase 2 of “Adhesives for Structural Joining” topic under the scheme of “A Joint Effort”, which is supported by Commonwealth of Australia as represented by Defence Science and Technology (DST Group) and Small Business Innovation Research for Defence (SBIRD), part of the Next Generation Technologies Fund. The authors acknowledge the facilities and the scientific and technical assistance of Microscopy Australia at the Electron Microscope Unit (EMU) within the Mark Wainwright Analytical Centre (MWAC) at UNSW Sydney.

Appendix A. Supplementary material

Supplementary data to this article can be found online at https://doi.org/10.1016/j.compositesa.2023.107597.

References

[1] Dennis CL, Ivkov R. Physics of heat generation using magnetic nanoparticles for hyperthermia. Int J Hyperth 2013;29:715–29. https://doi.org/10.3109/02656736.2013.836758.
[2] Zhang H, Lin B, Tang J, Wang Y, Wang H, Zhang H, et al. An ethyl cellulose-based supramolecular gel composite coating for metal corrosion protection and its self-healing property from electromagnetic heating effect. Surf Coatings Technol 2021;424:127647. https://doi.org/10.1016/j.surfcoat.2021.127647.
[3] Buckley JD, Fox RL. Rapid electromagnetic induction bonding of composites. Plastics Metals MRS Proc 1988;124:317. https://doi.org/10.1557/PROC-124-317.
[4] Jung K-C, Roh I-T, Chang S-H. Evaluation of mechanical properties of polymer concretes for the rapid repair of runways. Compos B Eng 2014;58:352–60. https://doi.org/10.1016/j.compositesb.2013.10.076.
[5] Cheng X, Zhou Y, Charles ADM, Yu Y, Islam MS, Peng S, et al. Enabling contactless rapid on-demand debonding and rebonding using hysteresis heating of ferrimagnetic nanoparticles. Mater Des 2021;210:110076. https://doi.org/10.1016/j.matdes.2021.110076.
[6] Johnston K, Pavuluri SK, Leonard MT, Desmulliez MPY, Arrighi V. Microwave and thermal curing of an epoxy resin for microelectronic applications. Thermochim Acta 2015;616:100–9. https://doi.org/10.1016/j.tca.2015.08.010.
[7] Yamazaki K, Fukushima N. Iron loss model for rotating machines using direct eddy current analysis in electrical steel sheets. IEEE Trans Energy Convers 2010;25:633–41. https://doi.org/10.1109/TEC.2010.2040179.
[8] Yu Q, Bilgin B, Emadi A. Loss and efficiency analysis of switched reluctance machines using a new calculation method. IEEE Trans Ind Electron 2015;62:3072–80. https://doi.org/10.1109/TIE.2015.2392716.
[9] Atkinson JR, Ward IM. The joining of biaxially oriented polyethylene pipes. Polym Eng & Sci 1989;29:1638–41. https://doi.org/10.1002/pen.760292303.
[10] Davies P, Cantwell WJ, Jar P-Y, Bourban P-E, Zysman V, Kausch HH. Joining and repair of a carbon fibre-reinforced thermoplastic. Composites 1991;22:425–31. https://doi.org/10.1016/0010-4361(91)90199-Q.
[11] Hou M, Friedrich K. Resistance welding of continuous glass fibre-reinforced polypropylene composites. Compos Manuf 1992;3:153–63. https://doi.org/10.1016/0956-7143(92)90078-9.
[12] Jongbloed B, Teuwen J, Palardy G, Villegas IF, Benedictus R. Continuous ultrasonic welding of thermoplastic composites: Enhancing the weld uniformity by changing the energy director. J Compos Mater 2020;54:2023–35. https://doi.org/10.1177/0021998319890405.

[13] Brito CBG, Teuwen J, Dransfeld CA, Villegas IF. The effects of misaligned adherends on static ultrasonic welding of thermoplastic composites. Compos A Appl Sci Manuf 2022;155:106810. https://doi.org/10.1016/j.compositesa.2022.106810.
[14] Wang Y, Rao Z, Liao S, Wang F. Ultrasonic welding of fiber reinforced thermoplastic composites: Current understanding and challenges. Compos A Appl Sci Manuf 2021;149:106578. https://doi.org/10.1016/j.compositesa.2021.106578.
[15] Sanders P. Electromagnetic welding: an advance in thermoplastics assembly. Mater Des 1987;8:41–5. https://doi.org/10.1016/0261-3069(87)90059-8.
[16] Xiang Z, Ducharne B, Della Schiava N, Capsal J-F, Cottinet P-J, Coativy G, et al. Induction heating-based low-frequency alternating magnetic field: High potential of ferromagnetic composites for medical applications. Mater Des 2019;174:107804. https://doi.org/10.1016/j.matdes.2019.107804.
[17] Rudolf R, Mitschang P, Neitzel M. Induction heating of continuous carbon-fibre-reinforced thermoplastics. Compos A Appl Sci Manuf 2000;31:1191–202. https://doi.org/10.1016/S1359-835X(00)00094-4.
[18] Ahmed TJ, Stavrov D, Bersee HEN, Beukers A. Induction welding of thermoplastic composites—an overview. Compos A Appl Sci Manuf 2006;37:1638–51. https://doi.org/10.1016/j.compositesa.2005.10.009.
[19] Bayerl T, Duhovic M, Mitschang P, Bhattacharyya D. The heating of polymer composites by electromagnetic induction – A review. Compos A Appl Sci Manuf 2014;57:27–40. https://doi.org/10.1016/j.compositesa.2013.10.024.
[20] Choudhury MR, Debnath K. A review of the research and advances in electromagnetic joining of fiber-reinforced thermoplastic composites. Polym Eng & Sci 2019;59:1965–85. https://doi.org/10.1002/pen.25207.
[21] Ciardiello R, Martorana B, Lambertini VG, Brunella V. Iron-based reversible adhesives: Effect of particles size on mechanical properties. Proc Inst Mech Eng Part C J Mech Eng Sci 2018;232:1446–55. https://doi.org/10.1177/0954406217736552.
[22] Ciardiello R, Belingardi G, Martorana B, Brunella V. Physical and mechanical properties of a reversible adhesive for automotive applications. Int J Adhes Adhes 2019;89:117–28. https://doi.org/10.1016/j.ijadhadh.2018.12.005.
[23] Salimi S, Babra TS, Dines GS, Baskerville SW, Hayes W, Greenland BW. Composite polyurethane adhesives that debond-on-demand by hysteresis heating in an oscillating magnetic field. Eur Polym J 2019;121:109264. https://doi.org/10.1016/j.eurpolymj.2019.109264.
[24] Saeed MB, Zhan M-S. Adhesive strength of partially imidized thermoplastic polyimide films in bonded joints. Int J Adhes Adhes 2007;27:9–19. https://doi.org/10.1016/j.ijadhadh.2005.12.001.
[25] Saeed MB, Zhan M-S. Adhesive strength of nano-size particles filled thermoplastic polyimides. Part-I: Multi-walled carbon nano-tubes (MWNT)–polyimide composite films. Int J Adhes Adhes 2007;27:306–18. https://doi.org/10.1016/j.ijadhadh.2006.06.001.
[26] Varley RJ, Charve F. EMAA as a healing agent for mendable high temperature epoxy amine thermosets. Compos A Appl Sci Manuf 2012;43:1073–80. https://doi.org/10.1016/j.compositesa.2012.01.018.
[27] Azevedo do Nascimento A, Fernandez F, da Silva FS, Ferreira EPC, Melo JDD, Cysne Barbosa AP. Addition of poly (ethylene-co-methacrylic acid) (EMAA) as self-healing agent to carbon-epoxy composites. Compos Part A Appl Sci Manuf 2020;137. https://doi.org/10.1016/j.compositesa.2020.106016.
[28] Meure S, Furman S, Khor S. Poly[ethylene-co-(methacrylic acid)] healing agents for mendable carbon fiber laminates. Macromol Mater Eng 2010;295:420–4. https://doi.org/10.1002/mame.200900345.
[29] Asadi J, Golshan Ebrahimi N, Razzaghi-Kashani M. Self-healing property of epoxy/nanoclay nanocomposite using poly(ethylene-co-methacrylic acid) agent. Compos A Appl Sci Manuf 2015;68:56–61. https://doi.org/10.1016/j.compositesa.2014.09.017.
[30] Hargou K, Pingkarawat K, Mouritz AP, Wang CH. Ultrasonic activation of mendable polymer for self-healing carbon–epoxy laminates. Compos B Eng 2013;45:1031–9. https://doi.org/10.1016/j.compositesb.2012.07.016.
[31] Yang T, Wang CH, Zhang J, He S, Mouritz AP. Toughening and self-healing of epoxy matrix laminates using mendable polymer stitching. Compos Sci Technol 2012;72:1396–401. https://doi.org/10.1016/j.compscitech.2012.05.012.
[32] Wang CH, Sidhu K, Yang T, Zhang J, Shanks R. Interlayer self-healing and toughening of carbon fibre/epoxy composites using copolymer films. Compos A Appl Sci Manuf 2012;43:512–8. https://doi.org/10.1016/j.compositesa.2011.11.020.
[33] Ciardiello R, Belingardi G, Litterio F, Brunella V. Effect of iron oxide and graphene particles on joint strength and dismounting characteristics of a thermoplastic adhesive. Int J Adhes Adhes 2021;107:102850. https://doi.org/10.1016/j.ijadhadh.2021.102850.
[34] Verwey EJW. Electronic conduction of magnetite (Fe3O4) and its transition point at low temperatures. Nature 1939;144:327–8. https://doi.org/10.1038/144327b0.
[35] Itai R, Shibuya M, Matsumura T, Ishi G. Electrical resistivity of magnetite anodes. J Electrochem Soc 1971;118:1709. https://doi.org/10.1149/1.2407817.
[36] Gozdur R, Gębara P, Chwastek K. A study of temperature-dependent hysteresis curves for a magnetocaloric composite based on La(Fe, Mn, Si)13-H type alloys. Energies 2020;13. https://doi.org/10.3390/en13061491.
[37] Xie W, Wang J, Berndt CC. Spreading Behavior and morphology of ethylene methacrylic acid (EMAA) deposits via the flame spray process. Coatings 2012;2. https://doi.org/10.3390/coatings2020076.
[38] Rahman SSU, Qureshi MT, Sultana K, Rehman W, Khan MY, Asif MH, et al. Single step growth of iron oxide nanoparticles and their use as glucose biosensor. Results Phys 2017;7:4451–6. https://doi.org/10.1016/j.rinp.2017.11.001.
[39] Veintemillas-Verdaguer S, del Puerto Morales M, Bomati-Miguel O, Bautista C, Zhao X, Bonville P, et al. Colloidal dispersions of maghemite nanoparticles produced by laser pyrolysis with application as NMR contrast agents. J Phys D Appl Phys 2004;37:2054–9. https://doi.org/10.1088/0022-3727/37/15/002.
[40] Mamunya YP, Davydenko VV, Pissis P, Lebedev EV. Electrical and thermal conductivity of polymers filled with metal powders. Eur Polym J 2002;38:1887–97. https://doi.org/10.1016/S0014-3057(02)00064-2.
[41] Zhou Y, Cheng X, Huang F, Sha Z, Han Z, Chen J, et al. Hierarchically structured electrodes for moldable supercapacitors by synergistically hybridizing vertical graphene nanosheets and MnO<inf>2</inf>. Carbon N Y 2021;172. https://doi.org/10.1016/j.carbon.2020.10.025.
[42] Cheng H, Wei S, Ji Y, Zhai J, Zhang X, Chen J, et al. Synergetic effect of Fe3O4 nanoparticles and carbon on flexible poly (vinylidence fluoride) based films with higher heat dissipation to improve electromagnetic shielding. Compos A Appl Sci Manuf 2019;121:139–48. https://doi.org/10.1016/j.compositesa.2019.03.019.
[43] Ayatollahi MR, Giv AN, Razavi SMJ, Khoramishad H. Mechanical properties of adhesively single lap-bonded joints reinforced with multi-walled carbon nanotubes and silica nanoparticles. J Adhes 2017;93:896–913. https://doi.org/10.1080/00218464.2016.1187069.
[44] De Cicco D, Asaee Z, Taheri F. Use of nanoparticles for enhancing the interlaminar properties of fiber-reinforced composites and adhesively bonded joints—A review. Nanomaterials 2017;7. https://doi.org/10.3390/nano7110360.
[45] Kim JW, Lee JS. The effect of the melt viscosity and impregnation of a film on the mechanical properties of thermoplastic composites. Mater (Basel, Switzerland) 2016;9:448. https://doi.org/10.3390/ma9060448.
[46] Koricho EG, Verna E, Belingardi G, Martorana B, Brunella V. Parametric study of hot-melt adhesive under accelerated ageing for automotive applications. Int J Adhes Adhes 2016;68:169–81. https://doi.org/10.1016/j.ijadhadh.2016.03.006.
[47] Ciardiello R, Belingardi G, Litterio F, Brunella V. Thermomechanical characterization of reinforced and dismountable thermoplastic adhesive joints activated by microwave and induction processes. Compos Struct 2020;244:112314. https://doi.org/10.1016/j.compstruct.2020.112314.
[48] Park Y-J, Joo H-S, Kim H-J, Lee Y-K. Adhesion and rheological properties of EVA-based hot-melt adhesives. Int J Adhes Adhes 2006;26:571–6. https://doi.org/10.1016/j.ijadhadh.2005.09.004.
[49] Heinzmann C, Coulibaly S, Roulin A, Fiore GL, Weder C. Light-induced bonding and debonding with supramolecular adhesives. ACS Appl Mater Interfaces 2014;6:4713–9. https://doi.org/10.1021/am405302z.
[50] Verna E, Cannavaro I, Brunella V, Koricho EG, Belingardi G, Roncato D, et al. Adhesive joining technologies activated by electro-magnetic external trims. Int J Adhes Adhes 2013;46:21–5. https://doi.org/10.1016/j.ijadhadh.2013.05.008.
[51] Muzakkar MZ, Ahmad S, Yarmo MA, Jalar A, Bijarimi M. Shear strength of single lap joint aluminium-thermoplastic natural rubber (Al-TPNR) laminated composite. J Phys Conf Ser 2013;423:12041. https://doi.org/10.1088/1742-6596/423/1/012041.
[52] Vattathurvalappil SH, Haq M. Thermomechanical characterization of Nano-Fe3O4 reinforced thermoplastic adhesives and single lap-joints. Compos B Eng 2019;175:107162. https://doi.org/10.1016/j.compositesb.2019.107162.